Interactive Virtual Humans: A Two-Level Prioritized Control Framework with Wrench Bounds

Mingxing Liu, Alain Micaelli, Paul Evrard, Adrien Escande, and Claude Andriot

Abstract—This paper presents a new control framework for virtual humans in a physics-based virtual environment. This framework combines multi-objective control with motion capture techniques. Each motion tracking task is associated with a task wrench. Bounds are imposed on lower-priority task wrenches to ensure the controller performance of higher-priority tasks. An optimization problem is solved to compute optimal task wrenches based on wrench bounds. Finally, joint torques are computed using the optimal task wrenches. The novelty of our wrench-bound method is that it can handle inequality constraints on a higher-priority task and maintain passivity as well. This control framework allows an operator to interact with the virtual human in real-time, without the necessity of compromising the virtual human's balance. It also allows the virtual human to generate appropriate motions to handle interactions with the virtual environment, rather than to simply emulate captured motions. The effectiveness of our approach is demonstrated by a virtual human performing reaching and manipulation tasks.

Index Terms—Virtual reality, Motion control, Task priority, Human robot interaction.

I. NOMENCLATURE

The following notation is adopted in this paper.

$\mathbf{M}$	generalized inertia matrix
$\mathbf{T}$	velocity in generalized coordinates
$\dot{\mathbf{T}}$	acceleration in generalized coordinates
$\mathbf{NT}$	centrifugal and Coriolis forces
γ	gravity force in generalized coordinates
$\mathbf{I}$	identity matrix
$\mathbf{L}$	matrix to select the actuated degrees of freedom (DoF) for a virtual human ($\mathbf{L} = \begin{bmatrix} \mathbf{0} & \mathbf{I} \end{bmatrix}^T$)
τ	the set of joint torques
$\mathbf{J}$	Jacobian matrix
$\mathbf{W}$	wrench applied by virtual humans on environments
$\mathbf{H}$	4×4 homogeneous transformation matrix
$\mathbf{R}$	rotation matrix
$\mathbf{X}$	position vector
$\mathbf{v}$	linear velocity
ω	angular velocity
$\mathbf{V}$	twist ($\mathbf{V} = [\mathbf{v}^T, \omega^T]^T$)
$tr()$	matrix trace

II. INTRODUCTION

Virtual humans (VHs), a form of simulated intelligent robots, usually need to interact with human operators and with virtual environments. They should react to operator's instructions and simulated events. Motion capture has become an essential technique in the control of VHs. It is traditionally used to guide the motions of a VH by virtual springs [1]. Many motion correction techniques based on pre-recorded motions [2]–[4] have shown good results, whereas our work studies real-time interactions where an operator can interact in an unpredictable way, such as during reaching or manipulation tasks in training environments or in industry design.

There are two main difficulties in this research topic. First, the operator's posture can be inappropriate for the VH, because the operator usually cannot sense forces applied on a VH during task execution. Consider the scenario where a VH pushes an obstacle; the operator just sends out the intention of pushing by reaching out his hands; but the VH may have to lean towards the obstacle to push it while the operator cannot, because the virtual obstacle does not exist in the world of the operator. Hence captured motions should be adjusted to be more suitable to handle external contact forces during interactions with the environment. Second, while multiple tasks are performed simultaneously, some tasks can be incompatible with one or another. Therefore, task conflicts have to be handled.

To address these problems, we investigate a two-level prioritized control framework, where multi-objective control is combined with motion capture techniques to retain the advantages of each. The VH is considered as a mechanical system influenced by multiple wrenches. The motion of each task frame is guided by its task wrench. Multiple tasks, as well as task priorities, are handled by regulating task wrenches. **Wrench bounds** are imposed on lower-priority task wrenches to ensure that they will not drive a higher-priority task frame out of its admissible domain.

The contributions of this work are as follows: 1) the development of a multi-objective control framework, which enables a VH to compromise between following an operator's motions, and deciding by itself how to perform tasks in a physics based virtual environment; 2) the development of a prioritized control approach based on wrench bounds, which allows inequality constraints on a higher-priority task, and takes into consideration the passivity of the system.

Part of this paper was presented in [5,6]. This paper extends [5] by describing in detail the wrench-bound method for handling task priorities. It is more general than [6] in that

it deals with not only reaching tasks, but also manipulation tasks; and it imposes bounds on task wrenches associated with motions in SE(3) (for special Euclidean group), rather than imposing constraints on task target positions in $\mathbb{R}^3$.

III. RELATED WORKS

A. Force-based control framework with optimization

Our control framework adopts a **Jacobian-transpose** (JT) control method, which has been used in [7] for virtual actuator control, and in [8] for a walking controller. The work in [9] reconstructed human motion from motion capture data, by using a simplified version of the framework proposed in [10]. This simplified version is close to the JT control method.

The principle of our control framework is similar to those presented in [11] and [12], both of which combined the JT method with optimization. The work in [11] proposed a static resolution of forces based on the relations of some action-reaction frame pairs. For each frame pair, a force variable applied at the action frame from the reaction frame is defined, as well as an opposite force variable applied at the reaction frame; then optimization is used to solve for these variables. Compared with such a method, ours is more general in the sense that it is not needed to identify action-reaction frame pairs. Each frame is associated with one force variable, so the number of optimization variables in our framework is the same as the number of task frames; however, if there are lots of body frames interacting with each other, the variable number becomes much larger with the method in [11]. Besides, contact constraints associated with friction cones were not considered in [11]. The work in [12] proposed a synthesis of control laws involving two main steps. The first step consists of estimating ground contact forces, which are used in the second step to compute joint torques by solving dynamics and constraint equations. These equations in the second step are solved by a damped pseudo-inverse, which leads to a solution that minimizes the norm of the vector $\begin{bmatrix} \dot{\mathbf{T}}^T & \tau^T \end{bmatrix}^T$. This may, in most situations, have the risk of generating unwanted behaviors or movements; for example, consider a simple gravity compensation, for which we do not want to move the VH at all, but the use of a damped pseudo-inverse may lead to $\dot{\mathbf{T}} \neq \mathbf{0}$.

B. Prioritized control with inequality constraints

A classical method to realize prioritized control is by using **null space projections** [10,13]–[15], in which a lower-priority task is satisfied only in the null space of higher-priority tasks. The null space projection ensures that lower-priority tasks are controlled without dynamically interfering with higher-priority tasks [16,17].

Inequality constraints on lower-priority tasks can be realized by the projection of an artificial potential field term [18] onto the null space of equality constraints, which proved especially efficient for task objectives such as joint limits or object avoidance [19,20]. A repulsive potential is used in [21] to keep the projected center of mass (CoM) away from the boundary of the support polygon, and the gradient of the potential is projected onto the null space of the hand task. But in this case, the CoM task is of lower-priority, so its controller performance can no longer be ensured. Moreover, when applying such a prioritization method, the higher-priority task frame will remain on its desired position, which can be too restrictive and may either reduce the workspace or result in more body movements in order to fulfill lower-priority tasks.

Instead of being constrained at a fixed position, a higher-priory task frame is sometimes allowed to move with a margin of error, within which the task performance can be ensured. Therefore, a prioritization method which allows inequality constraints at a higher-priority level is needed. Null space projector has been adopted in [22] to integrate unilateral constraints at any priority level. This approach has achieved impressive results, although the computation of some specific inverse operators is complex and time consuming. An alternative solution is to use **a sequence of quadratic programs** [23]–[26]. Such kind of prioritization process boils down to the classical algorithm based on null space projections when only linear equalities are considered [23]. All the methods mentioned here, among many others, rely on null space projections; but it is shown in [27,28] that prioritization based on projections can **break passivity**, which is a sufficient condition to guarantee stable operations [29,30].

To avoid breaking passivity, we propose to impose wrench bounds on lower-priority tasks, so as to guarantee that they are fulfilled only if their task wrenches will not drive a higher-priority task frame out of its admissible domain. This prioritized control can be adaptable to motion tracking tasks. Wrench bounds are computed automatically at each time step. There is no need to manually tune control parameters, such as weights or gains used in the optimization. Inequality constraints on a higher-priority task are allowed, which means the higher-priority task frame is allowed to move as long as the error remains within a tolerance margin. This provides lower-priority tasks with more freedom of movement, since they are to some extent allowed to dynamically interfere with a higher-priority task. The energy is bounded in our method, so the system is passive, since it cannot supply power indefinitely.

IV. DYNAMICS OF THE VIRTUAL HUMAN

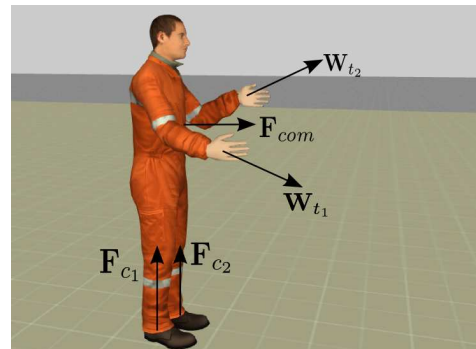The dynamics of the VH (Fig.1) is considered as a second order system (1).

Fig. 1. Example of a VH with wrenches associated with different frames.

$$\mathbf{M}\dot{\mathbf{T}} + \mathbf{N}\mathbf{T} + \gamma^r = \mathbf{L}\tau - \sum_j \mathbf{J}_{c_j}^T \mathbf{W}_{c_j}^r - \sum_k \mathbf{J}_{p_k}^T \mathbf{W}_{p_k}^r \quad (1)$$

In the notations of this paper, frames are denoted by subscripts as follows:

- *com* for CoM frame;
- *c* for non-sliding contacts at fixed locations, which are known a priori, such as the contacts between the feet and the ground;
- *p* for contacts where the environment is not fixed but behaves passively, which means that the VH experiences a passive interaction with the environment; these contacts are unknown a priori;
- *t* for task frames associated with the end-effector motion control.

Note that only passive interactions between the VH and the environment is considered here. The restriction to passive interactions is a natural choice, since the human can be supposed to behave like a passive environment [31], and a great number of environments with which people and robots interact are passive [32].

Moreover the following superscripts are used:

- *d* for "desired" wrench values for the controller,
- *r* for "real" wrench values in a simulation,
- *root* for the root DoF,
- *ac* for the actuated DoF,
- *t* for a value at time *t*.

With these notations, a Jacobian matrix $\mathbf{J}$ is decomposed as $\mathbf{J} = \begin{bmatrix} \mathbf{J}^{root} & \mathbf{J}^{ac} \end{bmatrix}$.

V. CONTROL FRAMEWORK

The control framework is shown in Fig. 2. At each time step of simulation, the control system computes joint torques from a motion capture sequence, given tasks, and constraints. The whole control is divided into two steps: the first step is the computation of the optimal wrenches; joint torques are then computed according to the optimal wrenches in the second step. The joint torques are used to drive the VH.

A. Virtual wrenches computation

First of all, the JT control method [7,9] is briefly reviewed here. Given a task wrench $\mathbf{W}$ in the space of Cartesian coordinates, the equivalent joint torques τ can be obtained by $\tau = \mathbf{J}^T\mathbf{W}$, with $\mathbf{J}$ the Jacobian matrix at the point where $\mathbf{W}$ is supposed to be applied.

In our multi-objective control, a task means that a certain frame on the VH's body should be transferred from an initial state to a desired state. For each task, imagine that a "virtual" wrench is applied at a certain frame on the VH's body to guide its motion towards a given target. These virtual wrenches are computed by solving an optimization problem.

The optimization variables are the CoM task force $\mathbf{F}_{com}$, the end-effector task wrenches $\mathbf{W}_{t_i}$, the contact forces $\mathbf{F}_{c_j}$, and the gravity force γ. The optimization tries to find optimal task wrenches by taking into account their desired values, the gravity compensation objective, as well as the constraints of static equilibrium, non-sliding contacts, and wrench bounds.
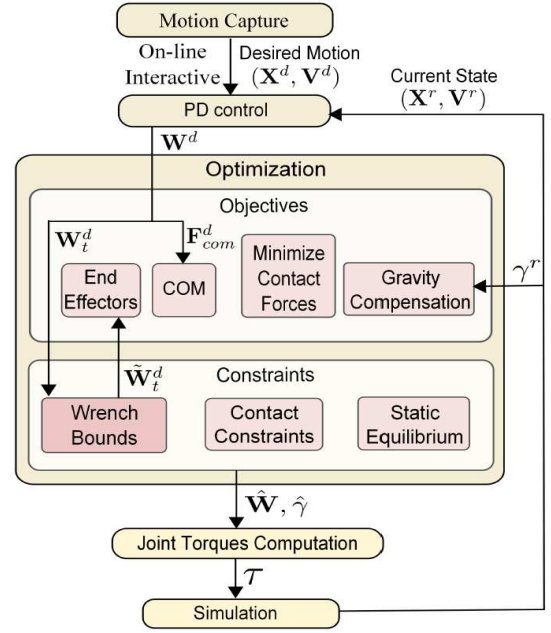

Fig. 2. Block diagram of the control framework.

Suppose there are n task frames for end-effector motion control and m fixed contacts. The optimization problem is written as follows:

$$\underset{\substack{\mathbf{F}_{com}, \mathbf{W}_{t_i}, \\ \mathbf{F}_{c_j}, \gamma}}{\arg\min} \quad \frac{1}{2} \left\| \begin{bmatrix} \mathbf{F}_{com}^d \\ \mathbf{W}_{t_i}^d \\ \mathbf{F}_{c_j}^d \\ \gamma^r \end{bmatrix} - \begin{bmatrix} \mathbf{F}_{com} \\ \mathbf{W}_{t_i} \\ \mathbf{F}_{c_j} \\ \gamma \end{bmatrix} \right\|_{\mathbf{Q}}^2 \quad (2a)$$

$$\text{subject to} \quad \mathbf{J}_{com}^{root\,T}\mathbf{F}_{com} + \sum_i \mathbf{J}_{t_i}^{root\,T}\mathbf{W}_{t_i}$$
$$+ \sum_j \mathbf{J}_{c_j}^{root\,T}\mathbf{F}_{c_j} + \gamma^{root} = 0 \quad (2b)$$
$$\mathbf{A}_{c_j}\mathbf{F}_{c_j} - \mathbf{d}_{c_j} > 0 \quad (2c)$$
$$\mathbf{W}_t^{min} \le \mathbf{W}_t \le \mathbf{W}_t^{max} \quad (2d)$$

with $i = 1, 2, ..., n$ and $j = 1, 2, ..., m$. The optimization objective is the same for each task, which is to minimize the error between the variable and its desired value. The objectives are combined by the diagonal weight matrix $\mathbf{Q}$, whose value is chosen according to the importance levels or the priorities of different objectives.

1) Target tracking objectives: The two primary kinds of target tracking tasks considered here are the CoM task and the end-effector tasks. Our control system takes the CoM as the stability criterion, and maintains balance by controlling its position. The end-effector tasks can be either tracking a captured motion sequence, or performing some specific motions. For each task, the desired task wrench $\mathbf{W}^d$ is computed by using a proportional-derivative (PD) feedback control law. For the end-effector tasks, both the position and orientation errors are considered; for the CoM task, only the position error is considered.

2) Contact force objective: For each fixed contact, only the force component $\mathbf{F}_{c_j}$ of the wrench $\mathbf{W}_{c_j}$ is considered. The contact force objective is not a target tracking objective. It is

used to minimize $\mathbf{F}_{c_j}$; so $\mathbf{F}_{c_j}^d$ is set to zero, as it is unknown a priori.

3) Gravity compensation objective: The purpose of this objective is to decouple the target tracking control with the existence of gravity into open-loop gravity compensation on one hand, and closed-loop correction of task errors on the other hand. Thus the PD gains for target tracking tasks can be set to lower values when the VH moves without the gravity disturbance. The desired value of the gravity force variable γ is the real gravity force γ^r.

4) Static equilibrium constraint: The wrenches are constrained by the static equilibrium of the root body under $\mathbf{F}_{com}$, $\mathbf{W}_{t_i}$, $\mathbf{F}_{c_j}$, and γ. This constraint is written in (2b).

5) Contact constraints: The objective in 2) only tries to minimize the contact forces $\mathbf{F}_{c_j}$, more appropriate values of which are computed by the optimization. The optimization searches for a contact force which not only satisfies the static equilibrium in 4), but also remains inside the friction cone, in order to maintain a non-sliding contact. The linearized Coulomb friction model [33,34] is applied, in which the friction cone of each contact is approximated by a four-faced polyhedral convex cone. The contact constraints are written in (2c), with

$$\mathbf{A}_{c_j} = \begin{bmatrix} \lambda_1 \times \lambda_2 & \lambda_2 \times \lambda_3 & \lambda_3 \times \lambda_4 & \lambda_4 \times \lambda_1 \end{bmatrix}^T, \quad (3)$$

where λ is the unit edge vector of the approximated friction cone; $\mathbf{d}_{c_j}$ is a user defined margin vector. The projection of $\mathbf{F}_{c_j}$ on the normal vector of each facet of the friction cone is constrained to be larger than $\mathbf{d}_{c_j}$.

6) Wrench bounds: Wrenches of lower-priority tasks are bounded if these tasks conflict with a higher-priority task. The constraint of wrench bounds has been mentioned in [5] without the description of how to compute them. In this paper, the computation of wrench bounds will be explained in detail in the next section.

B. Joint torques computation

Joint torques are computed in (4) using the solution ($\hat{\mathbf{F}}_{com}$, $\hat{\mathbf{W}}_{t_i}$, $\hat{\mathbf{F}}_{c_j}$, and $\hat{\gamma}$) of the optimization.

$$\tau = \mathbf{J}_{com}^{ac\ T}\hat{\mathbf{F}}_{com} + \sum_i \mathbf{J}_{t_i}^{acT}\hat{\mathbf{W}}_{t_i} + \sum_j \mathbf{J}_{c_j}^{acT}\hat{\mathbf{F}}_{c_j} + \hat{\gamma}^{ac}, \quad (4)$$

VI. WRENCH-BOUND METHOD

Our two-level prioritized control is realized by a wrench-bound method, which proposes to impose bounds on lower-priority task wrenches, so as to guarantee that a higher-priority task can be fulfilled.

To explain the idea of this method, suppose that there are w virtual wrenches, one of which is associated with a higher-priority task. Let $\mathcal{L}^+ = \{0, 1, 2, ..., w-1\}$ and $\mathcal{L} = \mathcal{L}^+ \backslash \{0\}$. The w wrenches are denoted as $\{\mathbf{W}_l : l \in \mathcal{L}^+\}$. The wrench associated with the higher-priority task is denoted as $\mathbf{W}_0$. Each lower-priority task wrench is denoted as $\mathbf{W}_l$ with $l \in \mathcal{L}$.

A. Preliminary conditions

This wrench-bound method is based on the following conditions:

- task targets are constant during each time step;
- an admissible domain exists for a higher-priority frame;
- the sum of the kinetic and potential energy at the initial time t_0 should be no larger than a threshold value $\mathbf{U}_0^{max}$, which will be defined later in this paper.

The admissible domain of a frame represents a tolerance margin around a desired configuration. The performance of a higher-priority task is ensured by constraining the task frame inside its admissible domain. For example, if the VH is standing on the horizontal ground, the admissible domain of the CoM should be defined in such a way that its vertical projection is inside the support polygon. The CoM should always lie inside its admissible domain to maintain balance. The bounds of lower-priority task wrenches should be found, which help to prevent them from driving the higher-priority frame out of its admissible domain.

B. The elastic potential energy associated with a wrench

The potential energy associated with a target position $\mathbf{X}_l^d$ has been used in [6] for the computation of constraints on translational movement. Such a method can be extended by defining a potential energy function $\mathbf{U}_l$ for each wrench $\mathbf{W}_l$ associated with a desired displacement $\mathbf{H}_l^d$. This potential energy $\mathbf{U}_l$ will be used later for the computation of wrench bounds.

The potential energy as a function of a body configuration $\mathbf{H}$ has been studied in [35], where the potential energy function is decomposed into translational, rotational, and coupling terms. The total potential energy is the sum of them. The coupling term is not considered here, so the total potential energy for $\mathbf{W}_l$ is defined as

$$\mathbf{U}_l(\mathbf{H}_l^d, \mathbf{H}_l) = \mathbf{U}_{l1}(\mathbf{X}_l^d, \mathbf{X}_l) + \mathbf{U}_{l2}(\mathbf{R}_l^d, \mathbf{R}_l), \quad (5)$$

where the translational potential energy $\mathbf{U}_{l1}$ is defined as

$$\mathbf{U}_{l1}(\mathbf{X}_l^d, \mathbf{X}_l) = \frac{1}{2}(\mathbf{X}_l^d - \mathbf{X}_l)^T\mathbf{K}_{l1}(\mathbf{X}_l^d - \mathbf{X}_l), \quad (6)$$

and the rotational potential energy $\mathbf{U}_{l2}$ is defined as

$$\mathbf{U}_{l2}(\mathbf{R}_l^d, \mathbf{R}_l) = tr(\mathbf{G}_l) - tr(\mathbf{G}_l\mathbf{R}_l^{-1}\mathbf{R}_l^d) \quad (7)$$

$$\mathbf{G}_l = \frac{1}{2}tr(\mathbf{K}_{l2})\mathbf{I} - \mathbf{K}_{l2} \quad (8)$$

with $\mathbf{K}_{l1}$ and $\mathbf{K}_{l2}$, the translational and the rotational part of the stiffness matrix $\mathbf{K}_l$ respectively, and $\mathbf{G}_l$, the co-stiffness matrix [35] associated with the stiffness matrix $\mathbf{K}_{l2}$. The term $tr(\mathbf{G}_l)$ is added to the form of the rotational potential energy defined in [35], so as to ensure the non-negative property of $\mathbf{U}_{l2}$ (see Appendix A). With the forms defined in (6) and (7), both $\mathbf{U}_{l1}$ and $\mathbf{U}_{l2}$ are non-negative; thus $\mathbf{U}_l(\mathbf{H}_l^d, \mathbf{H}_l)$ is non-negative.

In order to bound wrenches, a scale variable α_l is added into the potential energy function of each lower-priority task:

$$\mathbb{U}_l(\alpha_l, \mathbf{H}_l^d, \mathbf{H}_l) = \alpha_l\mathbf{U}_l(\mathbf{H}_l^d, \mathbf{H}_l), \ l \in \mathcal{L}. \quad (9)$$

For the sake of simplicity, $\mathbf{U}_l(\mathbf{H}_l^d, \mathbf{H}_l)$ will be denoted as $\mathbf{U}_l$ in the rest of this paper.

When $\mathbf{H}_0$ moves to the edge of its admissible domain, $\mathbf{U}_0$ increases to its maximum allowable value, denoted as $\mathbf{U}_0^{max}$.

The wrenches are associated with the potential:

$$\mathbf{W}_l = \begin{cases} -\nabla_{\mathbf{H}_l}\mathbf{U}_l - \mathbf{B}_l\mathbf{V}_l, \ l = 0, \\ -\alpha_l\nabla_{\mathbf{H}_l}\mathbf{U}_l - \mathbf{B}_l\mathbf{V}_l, \ l \in \mathcal{L}, \end{cases} \quad (10)$$

with $\mathbf{B}_l$ denoting the damping matrix, and the desired velocity $\mathbf{V}_l^d$ being set to zero. Here we abused the vector operator gradient to denote the differential of the potential energy function with respect to displacements in SE(3). The detail of its computation can be found in [35].

C. Wrench bounds computation

A VH is an under-actuated system, which needs to use contact forces to balance the wrenches due to task performance. Therefore, the wrench $\mathbf{W}_l$ given by the wrench-bound method should satisfy the following condition:

$\exists$ *contact forces* $\hat{\mathbf{F}}_{c_j}$: (i) *the static equilibrium* (11) *is satisfied;* (ii) *the non-sliding contact constraint* (2c) *is satisfied.*

$$\begin{cases} \mathbf{0} = \sum_l \mathbf{J}_l^{root^T}\mathbf{W}_l + \sum_j \mathbf{J}_{c_j}^{root^T}\hat{\mathbf{F}}_{c_j} + \hat{\gamma}^{root} & (11a) \\ \tau = \sum_l \mathbf{J}_l^{ac^T}\mathbf{W}_l + \sum_j \mathbf{J}_{c_j}^{ac^T}\hat{\mathbf{F}}_{c_j} + \hat{\gamma}^{ac} & (11b) \end{cases}$$

According to our experiences, the constraints (11) and (2c) can be satisfied for many tasks which do not require very fast motions. One possible reason for this is that task errors during each time step are small for slow motions, making the values of desired task wrenches not very large, so the tangential contact forces required to balance task wrenches will not need to be very large either. Therefore, we make the assumption that the wrench $\mathbf{W}_l$ given by the wrench-bound method satisfies both (11) and (2c). Moreover, the gravity force is assumed to be well estimated; thus the error between $\hat{\gamma}$ and γ^r is neglected in wrench bounds computation. Results of our experiments suggest that our method based on these assumptions works well. An investigation about the objective measure to assure slowness can be found in Appendix B.

Using the right members of (11a) and (11b) in the dynamics of the system (1) leads to

$$\mathbf{M}\dot{\mathbf{T}} + \mathbf{N}\mathbf{T} = \begin{bmatrix} \sum_l \mathbf{J}_l^{root^T}\mathbf{W}_l + \sum_j \mathbf{J}_{c_j}^{root^T}\hat{\mathbf{F}}_{c_j} + \hat{\gamma}^{root} \\ \sum_l \mathbf{J}_l^{ac^T}\mathbf{W}_l + \sum_j \mathbf{J}_{c_j}^{ac^T}\hat{\mathbf{F}}_{c_j} + \hat{\gamma}^{ac} \end{bmatrix}$$
$$- \sum_j \mathbf{J}_{c_j}^T\mathbf{F}_{c_j}^r - \sum_k \mathbf{J}_{p_k}^T\mathbf{W}_{p_k}^r - \gamma^r$$
$$= \sum_l \mathbf{J}_l^T\mathbf{W}_l - \sum_k \mathbf{J}_{p_k}^T\mathbf{W}_{p_k}^r + \sum_j \mathbf{J}_{c_j}^T(\hat{\mathbf{F}}_{c_j} - \mathbf{F}_{c_j}^r). \tag{12}$$

Separating the higher-priority task 0 from the others yields

$$\mathbf{M}\dot{\mathbf{T}} + \mathbf{N}\mathbf{T} = \mathbf{J}_0^T\mathbf{W}_0 + \sum_{l \in \mathcal{L}} \mathbf{J}_l^T\mathbf{W}_l$$
$$- \sum_k \mathbf{J}_{p_k}^T\mathbf{W}_{p_k}^r + \sum_j \mathbf{J}_{c_j}^T(\hat{\mathbf{F}}_{c_j} - \mathbf{F}_{c_j}^r). \tag{13}$$

After some computations, the energy with respect to time $t \in [t_0, t_0 + T]$ can be obtained from the following relation. The details of the computations can be found in Appendix C.

$$\mathbf{E}^{t_0} - \mathbf{E}^{t_0+T} - \int_{t_0}^{t_0+T} \mathbf{D}^t dt$$
$$= \mathbf{U}_0^{t_0+T} - \mathbf{U}_0^{t_0} - \int_{t_0}^{t_0+T} \mathbf{V}_0^{d,t^T}\nabla_{\mathbf{H}_0^{d,t}}\mathbf{U}_0^t dt$$
$$+ \sum_{l \in \mathcal{L}} (\alpha_l^{t_0+T}\mathbf{U}_l^{t_0+T} - \alpha_l^{t_0}\mathbf{U}_l^{t_0})$$
$$- \int_{t_0}^{t_0+T} \sum_{l \in \mathcal{L}} (\dot{\alpha}_l^t\mathbf{U}_l^t + \alpha_l^t\mathbf{V}_l^{d,t^T}\nabla_{\mathbf{H}_l^{d,t}}\mathbf{U}_l^t)dt$$
$$+ \int_{t_0}^{t_0+T} \sum_k \mathbf{V}_{p_k}^{t^T}\mathbf{W}_{p_k}^{r,t}dt, \tag{14}$$

with

$$\mathbf{D}^t = \mathbf{T}^{t^T}(\mathbf{J}_0^{t^T}\mathbf{B}_0\mathbf{J}_0^t + \sum_{l \in \mathcal{L}} \mathbf{J}_l^{t^T}\mathbf{B}_l\mathbf{J}_l^t)\mathbf{T}^t,$$
$$\mathbf{E}^t = \int_{t_0}^t (\mathbf{T}^{t^T}\mathbf{M}^t\dot{\mathbf{T}}^t + \mathbf{T}^{t^T}\mathbf{N}^t\mathbf{T}^t)dt, \tag{15}$$

where $\mathbf{D}$ is for dissipation. By using integration by parts, and noting that $\dot{\mathbf{M}} - 2\mathbf{N}$ is skew-symmetric [36], the expression of $\mathbf{E}^t$ in (15) gives the kinetic energy at time t.

Let $\mathbf{\Phi}$ denote the sum of the kinetic and potential energy. According to [29], the term $\int_{t_0}^{t_0+T} \sum_k \mathbf{V}_{p_k}^{t^T}\mathbf{W}_{p_k}^{r,t}dt$ should be non-negative for a passive interaction. Applying this property in (14) yields

$$\mathbf{\Phi}^{t_0+T} \le \mathbf{\Phi}^{t_0} + \mathbf{\Lambda}^{t_0+T}, \tag{16}$$

with

$$\mathbf{\Phi}^t = \mathbf{E}^t + \mathbf{U}_0^t + \sum_{l \in \mathcal{L}} \alpha_l^t\mathbf{U}_l^t,$$
$$\mathbf{\Lambda}^t = \int_{t_0}^t \dot{\mathbf{\Lambda}}^t dt,$$
$$\dot{\mathbf{\Lambda}}^t = \sum_{l \in \mathcal{L}} (\dot{\alpha}_l^t\mathbf{U}_l^t + \alpha_l^t\mathbf{V}_l^{d,t^T}\nabla_{\mathbf{H}_l^{d,t}}\mathbf{U}_l^t)$$
$$+ \mathbf{V}_0^{d,t^T}\nabla_{\mathbf{H}_0^{d,t}}\mathbf{U}_0^t - \mathbf{D}^t. \tag{17}$$

In order to maintain the higher-priority frame inside its admissible domain, the total energy $\mathbf{\Phi}^t$ is constrained to be no larger than $\mathbf{U}_0^{max}$, the maximum allowed value of $\mathbf{U}_0$:

$$\mathbf{\Phi}^t \le \mathbf{U}_0^{max}, \ \forall t \in [t_0, t_0 + T]. \tag{18}$$

Moreover, the potential energy should be non-negative, so α_l should be non-negative. These constraints lead to the following constraint for each α_l at initial time:

$$0 \le \alpha_l^{t_0} \le \frac{\mathbf{U}_0^{max} - \mathbf{U}_0^{t_0} - \mathbf{E}^{t_0}}{\sum_{l \in \mathcal{L}} \mathbf{U}_l^{t_0}}, \tag{19}$$

which is a sufficient condition for (18). Note that according to the third preliminary condition mentioned in VI-A, we have $\mathbf{\Phi}^{t_0} \le \mathbf{U}_0^{max}$, which ensures that the upper bound of $\alpha_l^{t_0}$ in (19) is non-negative.

Once we have $\alpha_l^{t_0}$ which satisfies (19), we now try to increase its value during the simulation, as long as (18) is satisfied. To realize this, we first try to increase $\mathbf{\Lambda}^t$, $\forall t \in$

$(t_0, t_0 + T]$. The following sufficient condition for (18) is applied by using (16):

$$\boldsymbol{\Phi}^t \leq \boldsymbol{\Phi}^{t_0} + \boldsymbol{\Lambda}^t \leq \mathbf{U}_0^{max}, \ \forall t \in (t_0, t_0 + T]. \qquad (20)$$

This relation leads to the following constraint on $\boldsymbol{\Lambda}^t$:

$$\boldsymbol{\Lambda}^t \leq \mathbf{U}_0^{max} - \boldsymbol{\Phi}^{t_0}, \ \forall t \in (t_0, t_0 + T], \qquad (21)$$

which gives an upper limit for $\boldsymbol{\Lambda}^t$. To satisfy (21) while trying to increase $\boldsymbol{\Lambda}^t$, $\dot{\boldsymbol{\Lambda}}^t$ is constrained as follows:

$$\dot{\boldsymbol{\Lambda}}^t \leq k_t(\mathbf{U}_0^{max} - \boldsymbol{\Phi}^{t_0} - \boldsymbol{\Lambda}^t), \ \forall t \in (t_0, t_0 + T], \qquad (22)$$

with k_t a positive gain parameter that regulates the rate of the increase of $\boldsymbol{\Lambda}^t$. Substituting $\dot{\boldsymbol{\Lambda}}^t$ in (22) with its expression in (17) yields

$$\sum_{l \in \mathcal{L}} \dot{\alpha}_l^t \mathbf{U}_l^t \leq \beta^t \qquad (23)$$

with

$$\beta^t = k_t(\mathbf{U}_0^{max} - \boldsymbol{\Phi}^{t_0} - \boldsymbol{\Lambda}^t) - \mathbf{V}_0^{d,t^T} \nabla_{\mathbf{H}_0^{d,t}} \mathbf{U}_0^t$$
$$+ \mathbf{D}^t - \sum_{l \in \mathcal{L}} \alpha_l^t \mathbf{V}_l^{d,t^T} \nabla_{\mathbf{H}_l^{d,t}} \mathbf{U}_l^t,$$

for which, the following sufficient condition is applied:

$$\dot{\alpha}_l^t \leq \frac{\beta^t}{\sum_{l \in \mathcal{L}} \mathbf{U}_l^t}. \qquad (24)$$

The relation (24) gives an upper limit of $\dot{\alpha}_l^t$.

Finally, based on (19) and (24), the bounded wrench for each lower-priority task is

$$\mathbf{W}_l = -\alpha_l \nabla_{\mathbf{H}_l} \mathbf{U}_l - \mathbf{B}_l \mathbf{V}_l, \ l \in \mathcal{L}, \qquad (25)$$

with α_l satisfying:

$$\begin{cases} 0 \leq \alpha_l^{t_0} \leq \min(\dfrac{\mathbf{U}_0^{max} - \mathbf{U}_0^{t_0} - \mathbf{E}^{t_0}}{\sum_{l \in \mathcal{L}} \mathbf{U}_l^{t_0}}, \alpha_l^{max}), & (26a) \\[3ex] \dot{\alpha}_l^t \leq \min[\dot{\alpha}_l^{max}, k_\alpha(\alpha_l^{max} - \alpha_l^t), \dfrac{\beta^t}{\sum_{l \in \mathcal{L}} \mathbf{U}_l^t}], & (26b) \\[3ex] \text{and } \alpha_l^t \geq 0, \ \forall t \in (t_0, t_0 + T], & (26c) \end{cases}$$

where α_l^{max} and $\dot{\alpha}_l^{max}$ are used to limit the upper limits of α_l and $\dot{\alpha}_l$; and k_α is a gain parameter whose value is user defined. In practice, we choose a value for α_l, which satisfies (26a) at the initial time. Then during the simulation, we use (26b) to try to increase α_l, and at the same time, to maintain the higher-priority frame inside its admissible domain.

The bounded wrenches will be used as on one hand, the new desired wrenches $\tilde{\mathbf{W}}^d$ in the optimization objectives, and on the other hand, the wrench bounds in the optimization constraints, as is illustrated in Fig.2.

VII. RESULTS

The proposed control framework has been implemented on a VH, who has a mass of $79kg$, and consists of 45 DoFs, with 6 DoFs for the root position and orientation, 8 DoFs for each leg, 7 DoFs for each arm, 3 DoFs for the thorax, 3 DoFs for the chest, and 3 DoFs for the head. There are four contact points on each foot. The control has been realized in real-time with a simulation time step of $0.01s$.

The CoM task is used for balance control; the hand tasks are used for reaching or manipulation control. It is strongly suggested to set a large weight for the gravity compensation objective, so as to enforce the estimated value of the gravity force be close to the real one.

The CoM task is chosen as a higher-priority task. The hand task wrenches are bounded to prevent them from driving the CoM out of its admissible domain. The desired CoM position $\mathbf{X}_{com}^d$ is limited by its maximum and minimum values: x^{min}, x^{max}, y^{min}, y^{max}, z^{min}, and z^{max}. There are different ways to define the CoM admissible domain, according to the desired CoM position, its limits, and the hand task targets. Two examples are given in Fig.3. In our experiments, the way described in Fig.3 (b) was adopted. The reference frame is defined as follows: the x axis points to the right, the y axis points to the front, and the z axis is determined by the right hand rule. The CoM is inside its admissible domain at the beginning of each simulation.

A. Reaching

In order to test our wrench-bound method, the VH was assigned with different reaching tasks. It was required to reach out for some objects with its hands but without moving its feet. The objects were either out of the VH's reach (Fig.4 left and middle) or on the ground (Fig.4 right). The objects situated out of the VH's reach were used to see if the hand task wrenches can be sufficiently bounded, so as to prevent the VH from falling down towards these objects. Our method was also tested with objects on the ground, since the CoM can easily move out of its admissible domain during a movement of crouching down.

The results with or without the application of wrench bounds, including the norm of the task force of the right hand, and the projection of the CoM position on the ground, are depicted in Fig.5. These results suggest that our wrench-bound
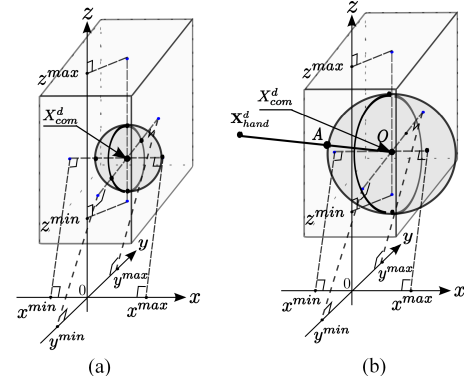

(a)   (b)

Fig. 3. Examples of the CoM admissible domain (the shaded ball). The maximum and minimum values of the CoM position form a cube. The boundary of the admissible domain is a sphere, with the origin O at $\mathbf{X}_{com}^d$. In (a), the sphere is inscribed in the cube. In (b), the radius of the sphere is the length of the line OA starting from $\mathbf{X}_{com}^d$ and pointing towards the hand task target $\mathbf{X}_{hand}^d$. The point A is the intersection point between OA and the cube. If the CoM is very close to x_{max}, then the admissible domain in (a) is very small. In fact, if the hand task will draw the CoM towards the direction of x_{min}, then a bigger admissible domain as in (b) can be used.
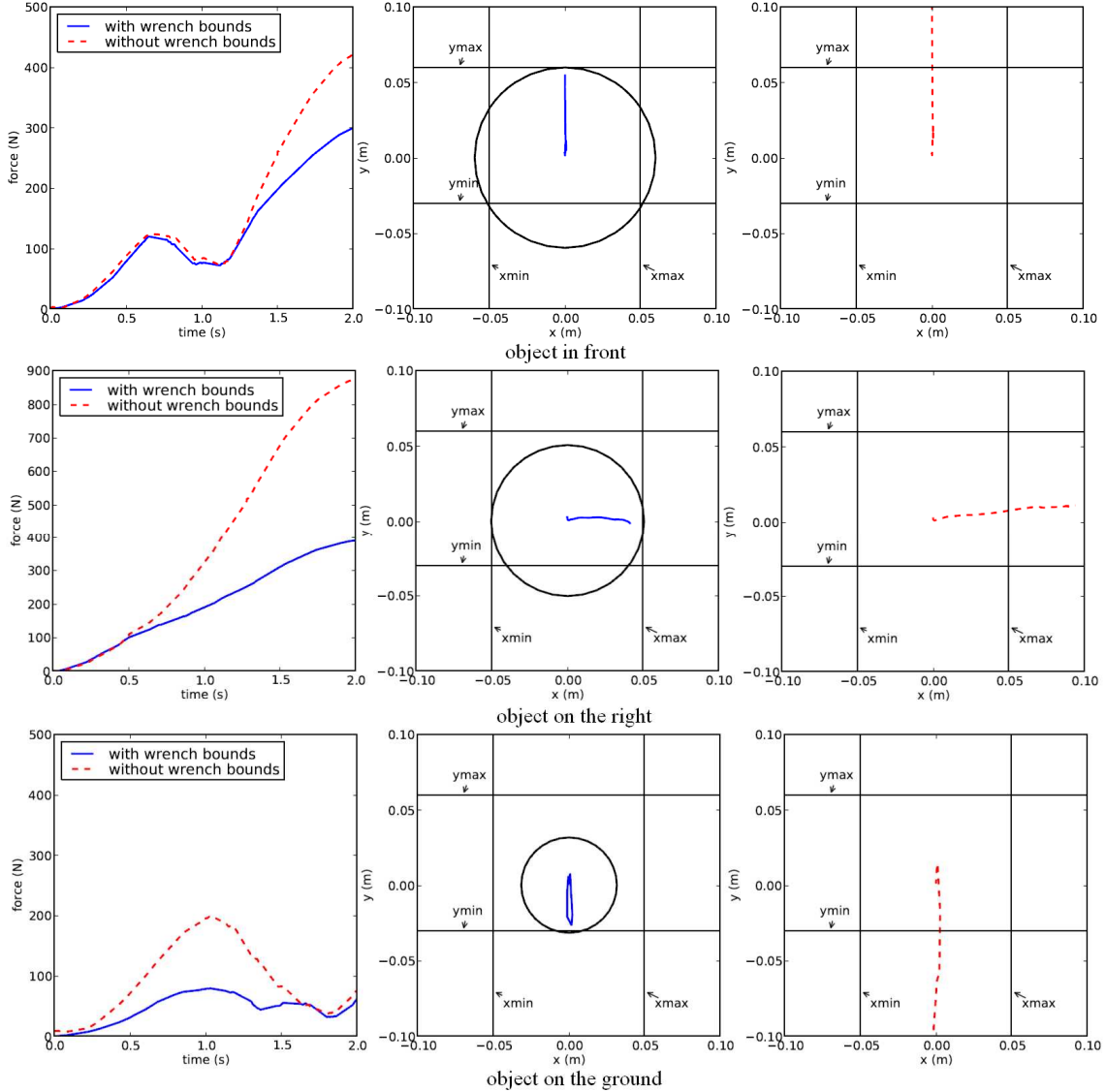
Fig. 5. Results of reaching for different objects: the norm of the task force of the right hand (left), the CoM position using wrench bounds (middle) and not using wrench bounds (right). The reference trajectory of each hand task is an interpolated trajectory from the initial to the target hand configuration. The admissible domains are shown by the circles.

method can successfully ensure the controller performance of a higher-priority task. Without the constraint of wrench bounds, the norm of the hand task force can be very large. Consequently, the hand task force can drive the VH too strongly, so that it leans too much towards the objects and its CoM may move out of the allowed domain. However, with wrench bounds applied on the hand task, the CoM can remain inside the admissible domain throughout the task.

The desired value of each optimization variable was compared with its value found by the optimization. To save space, we only depict the results during reaching out for an object in front, including the task wrench of the right hand (see Fig.6) and the gravity force γ (see Fig.7). It can be seen that the optimization solution of each variable is very close to its desired value.

B. Object manipulation through interaction with an operator

Two more sophisticated experiments were conducted, where the VH was required to turn a lever and a tap through interaction with an operator (Fig.8). The objects to manipulate were on the ground and it was necessary to crouch down to reach them. Moreover, these objects existed only in the virtual environment instead of in the real world of the operator.

During human-VH interactions, the VH was animated according to the hand displacements of the operator, which were captured in real-time and taken as the reference hand displacements for the VH. Once the VH achieved to grasp the object, it should start to perform manipulation according to the guidance of the operator's motions. Only the motions of the operator's hands were captured; the motions of the whole body of the VH were generated by the control system.

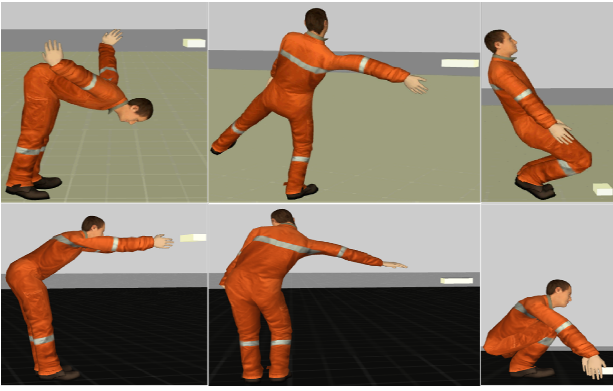In the experiments, when the desired value of hand task

Fig. 4. Snapshots of the VH performing reaching tasks without wrench bounds (above) and with wrench bounds (below). The upper part of the figure shows how the tasks are poorly performed without the application of wrench bounds. The VH loses its balance for the reaching task to be fulfilled. The lower part shows that, when wrench bounds are applied on hand tasks, the VH can keep its balance while trying to reach out for the objects.
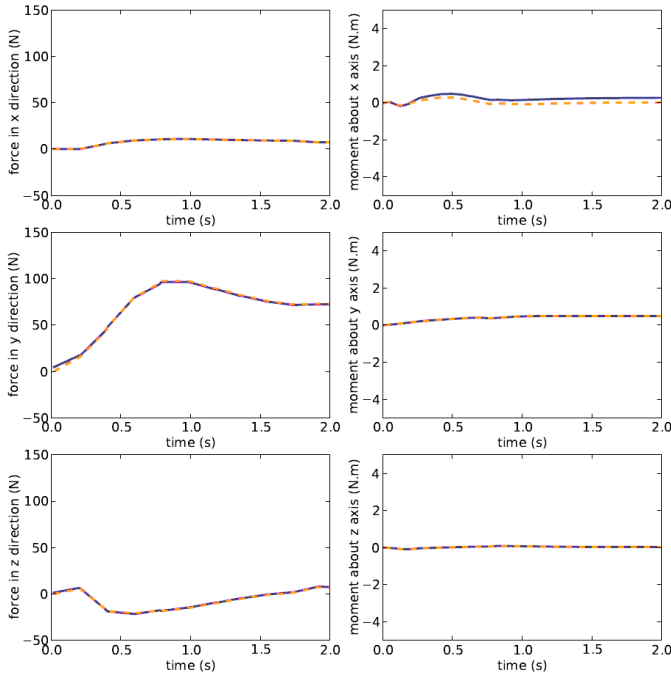

Fig. 6. The desired hand task wrench $\tilde{\mathbf{W}}^d$ with the application of wrench bounds (dark blue lines) during reaching out for an object in front, and the optimization solution $\hat{\mathbf{W}}$ (orange dashed lines).

Fig. 7. The real gravity force γ^r (dark blue lines) during reaching out for an object in front, and the optimization solution $\hat{\gamma}$ (orange dashed lines). To save space, only the elements corresponding to the DoFs of the root are depicted.

VIII. DISCUSSION

A. Verification of the assumption

We have assumed in VI-C that for many tasks which do not require very fast motions, the wrenches given by the wrench-bound method can satisfy the optimization constraints, and contact forces satisfying these constraints can be found. This assumption can be verified by comparing the bounded desired values of the optimization variables with their optimization results, since the former should be equal to the latter if what we have assumed is true. The experimental results, for example those in Fig.6 and Fig.7, show that the desired values are very close to the optimization results. This suggests that the assumption works well during the experiments.

For motions where the contact constraint (2c) can be violated, such as some fast motions, this assumption does not work well, and the passivity of the system may not be guaranteed. Future work should find a way to early predict and avoid such situations.

B. Shared control

The experiments suggest that the proposed control framework can successfully control the VH to perform manipulation tasks through interaction with an operator (Fig.8). During human-VH interaction, the computer and the human operator share their control on the VH. The operator sends higher-level task indications; the controller handles these tasks from a lower-level to respect the operator's intentions as much as possible. Such mode is sometimes referred to as shared control or human-in-the-loop [37]. In our shared control, the operator may not be able to provide an appropriate posture

wrenches were not bounded in the optimization, the VH could lose balance from time to time. The reasons for this are, on one hand, a movement of crouching down requires great changes in posture, as a result, the CoM position can often be too close to or even out of its admissible domain, as is shown in Fig.5 below; on the other hand, the interaction forces due to object manipulations can perturb the motions of the CoM. However, when bounds were imposed on hand task wrenches, the CoM movements were restricted throughout the manipulation. The VH successfully moved its body to manipulate the objects without losing balance. The real-time animation can be seen in the accompanying video.
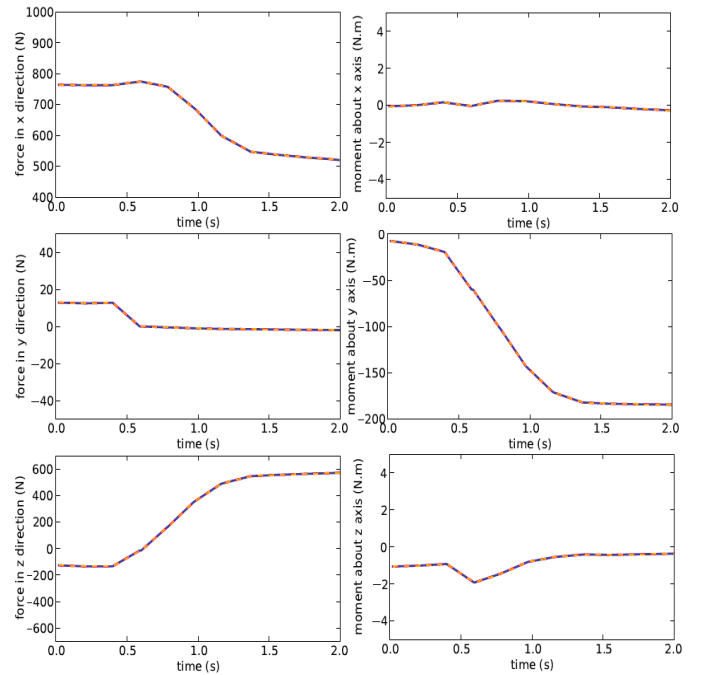
for a manipulation task, since the operator cannot really apply forces on a virtual object; however, by taking account of all the objectives and constraints in the optimization, the controller can adjust captured motions to handle interactions with the virtual environment. The balance of the VH is ensured when the CoM task is assigned with a higher priority than all the other motion tracking tasks. As a result, the VH can move the end-effector in its reachable space safely, and try its best to track the captured motions. An advantage of our approach is that the operator can provide any reference motion to guide the VH, without being worried about the VH's balance problem.

C. The choice of control parameters

For many prioritized control using optimization techniques, the control parameters such as task gains should be chosen very carefully, since they can affect the relative performances between tasks of different priority levels. Even though some gains can work for the tracking of one reference position, they might not be suitable for another one. In other words, it is difficult to manually find task gains that can ensure prioritization satisfactorily for a whole reference trajectory. This problem becomes more obvious during real-time interactions with an operator, where the VH is continuously tracking the motions of the operator's hands that can be anywhere in the operator's reachable space, and it is undesirable to manually tune these parameters for the whole reachable space. Yet automated optimization of gains to ensure task priorities has not been realized in many existing approaches. Our experiments suggest that the proposed wrench-bound approach can handle such problem. In the proposed wrench-bound approach, the control gain $\mathbf{K}_l$ of a lower-priority task is not fixed, on the contrary, it is automatically adjusted on-line by multiplying it with α_l for a better task performance according to the state of the system. An example is shown in Fig.9, where the hand task gain is automatically adjusted.

In our control framework, the weight of contact force objective is set to 1; and the weight of gravity compensation objective takes the highest value, which was 10^4 in our experiments. The weights associated with target tracking objectives can simply be chosen according to their importance levels. The least important one is assigned with a weight of 100. If the importance of task m is one level higher than the importance of task n, then the weight of task m is increased to 10 times the weight of task n. In fact, by applying wrench bounds, the weights of tracking task objectives will no longer affect the performance of prioritization (see Fig.9).

D. Comparison with some other approaches

In our approach, the priority of the CoM task over the hand tasks is realized by imposing bounds on hand task wrenches. In fact, the hand task wrenches are bounded by the control of the gains. If the hand task wrench can drive the CoM out of its admissible domain, then the proportional gain of the hand task is reduced to a safe value. It is also possible to handle task priorities by other two different approaches as follows:

- *Approach I*: Constraining the CoM to be within its admissible domain by applying a CoM task force derived from a repulsive potential field. If the CoM is close to the boundary of its admissible domain, then the repulsive force will pull it back.
- *Approach II*: Null-space projection methods.

Approach I is more simplistic compared with our approach. However, the use of a repulsive potential to constrain the CoM may result in a high CoM task gain. In a simulated environment, the sampling frequency is limited; therefore, a high CoM task gain may lead to unstable motions. This is why our approach decreases the gains of lower-priority tasks, instead of increasing the gain of the higher-priority task.

Approach II is a classical method to handle tasks with different priorities. Our approach realizes prioritized control by a quite different way from *Approach II*. The major differences between the two approaches are as follows: a) Our wrench-bound based control framework provides a quasi-static control; whereas *Approach II* can be dynamically consistent, and it requires the knowledge of the accurate dynamic model of the system. b) The current wrench-bound approach handles task priorities of two levels; while *Approach II* can handle more priority levels. c) As is mentioned before, the passivity of the system is respected by our approach; while projections may cause a risk of breaking the passivity. d) Our optimization based control framework can easily implement the non-sliding contact constraint (2c). One can verify if a contact force is inside a friction cone with projection based methods, such as [38]; but [38] does not mention how the non-sliding contact constraint is taken into account in the control. e) Our prioritized control allows inequality constraints on a higher-priority task, so the constraint on the CoM task can be less restrictive. This means that instead of being constrained to one desired position, the CoM is allowed to be interfered with a lower-priority task, as long as it remains inside an admissible domain. However, in *Approach II*, lower-priority tasks are not allowed to interfere with higher-priority tasks; as a result, more body movements may be needed to fulfill given tasks.

Our approach has been compared with *Approach II* by some experiments, in which the VH was performing reaching tasks. The controller in [10] was used to implement *Approach II*. The same tasks, task priorities, as well as task targets, were used in both approaches. These tasks from the highest priority to the lowest priority were: the foot contacts, the CoM, and the hands. The foot contacts were treated as optimization constraints in our approach.

It was observed that, when controlled by our approach or *Approach II*, the VH behaved similarly in most cases, but differently when mechanical interactions with the environment occurred during task execution. To simulate a mechanical interaction, the VH's right arm was connected with an object by an elastic Cartesian string (Fig. 10). A sudden perturbation force was applied on its arm by pulling the object. Note that the perturbation was not strong enough to pull the CoM out of its admissible domain. The reaching behaviors of the VH controlled by both approaches were similar before the perturbation. After the perturbation, a lot more body movements were generated with *Approach II*. The whole body rotated and the right arm actively pulled the string. This can be because the hand tasks were not allowed to interfere with the CoM task
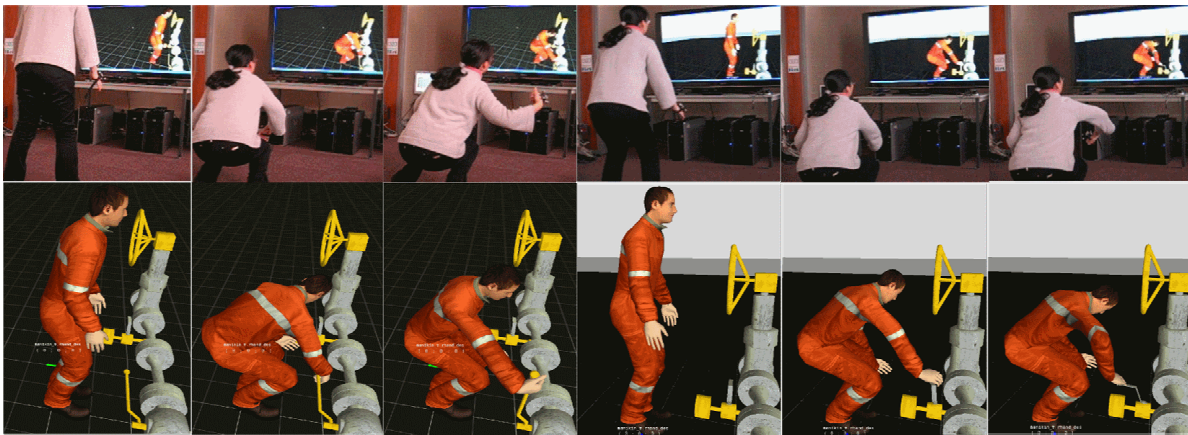
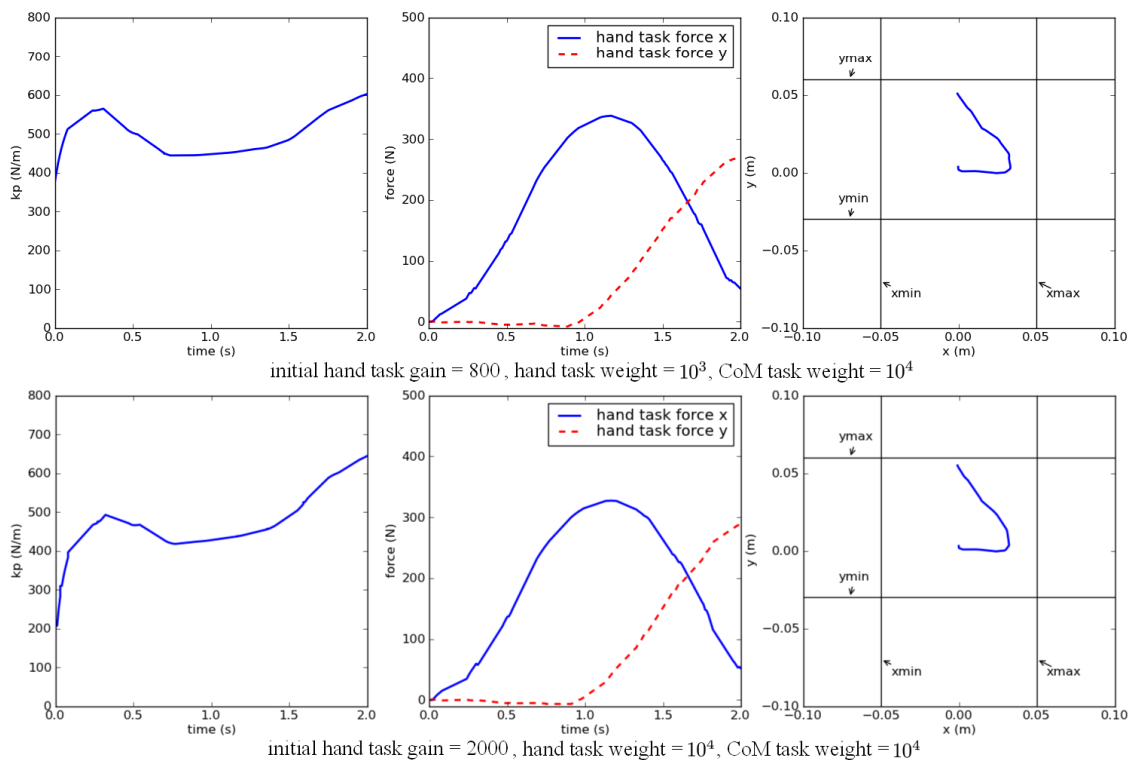Fig. 8. Snapshots of the VH manipulating a lever and a tap.

initial hand task gain = 800, hand task weight = 10^3, CoM task weight = 10^4

initial hand task gain = 2000, hand task weight = 10^4, CoM task weight = 10^4

Fig. 9. Results using different hand task weights and initial gains: the bounded proportional gain $\mathbf{K}_l$ of the hand tasks (left), the bounded hand task force (middle), and the CoM Position (right). To save space, only the elements corresponding to the translational movements of the right hand are depicted. The task is to first reach for an object at $1.2m$ on the right with the right hand during $1s$, then reach for another one at $1.2m$ in front with both hands during $1s$. The bounded task gain varies according to system states during task execution. The CoM remains inside its admissible domain, and the CoM task is allowed to be interfered with hand tasks. The results of prioritization are stable with respect to different choices of initial gains or weights.

when the VH was trying to compensate for the perturbation. The simulation can be seen in the video.

IX. CONCLUSIONS

A novel control framework for virtual humans, which combines prioritized multi-objective control with motion capture techniques, is presented. The wrench-based control policy allows the VH to be adapted to unknown external contact forces, and handle unilateral constraints on contact forces; therefore, the controller can generate motions suitable in a

virtual environment, rather than simply emulating captured motions.

The proposed wrench-bound method provides a new way to handle two-level task priorities. Such method allows inequality constraints on a higher-priority task, so lower-priority tasks are allowed to interfere with a higher-priority task. Moreover, the passivity of the system has been taken care of to ensure stable operations. As a result, the VH can keep the higher-priority task frame inside an admissible domain while trying its best to increase the performance of lower priority tasks in a safe manner.

of $u = [u_x u_y u_z]^T$, written as follows:

$$\mathbf{R} = \begin{bmatrix} c_\theta + u_x^2 \bar{c}_\theta & u_x u_y \bar{c}_\theta - u_z s_\theta & u_x u_z \bar{c}_\theta + u_y s_\theta \\ u_y u_x \bar{c}_\theta + u_z s_\theta & c_\theta + u_y^2 \bar{c}_\theta & u_y u_z \bar{c}_\theta - u_x s_\theta \\ u_z u_x \bar{c}_\theta - u_y s_\theta & u_z u_y \bar{c}_\theta + u_x s_\theta & c_\theta + u_z^2 \bar{c}_\theta \end{bmatrix}$$
$$(28)$$

with $c_\theta = cos\theta$, $s_\theta = sin\theta$ and $\bar{c}_\theta = 1 - cos\theta$.

With these notations, the rotational potential energy can be written as

$$\begin{aligned} \mathbf{U}_{l2} &= tr(\mathbf{G}_l) - tr(\mathbf{G}_l \mathbf{R}) \\ &= (g_1 + g_2 + g_3) \\ &\quad - (g_1(c_\theta + u_x^2 \bar{c}_\theta) + g_2(c_\theta + u_y^2 \bar{c}_\theta) + g_3(c_\theta + u_z^2 \bar{c}_\theta)) \\ &= (g_1 + g_2 + g_3 - g_1 u_x^2 - g_2 u_y^2 - g_3 u_z^2)\bar{c}_\theta \end{aligned}$$
$$(29)$$

Since u is a unit vector, we have $u_x^2 + u_y^2 + u_z^2 = 1$. Applying this in (29) leads to

$$\mathbf{U}_{l2} = (g_1(u_y^2 + u_z^2) + g_2(u_z^2 + u_x^2) + g_3(u_x^2 + u_y^2))\bar{c}_\theta \quad (30)$$

Then applying (27) in (30) leads to

$$\mathbf{U}_{l2} = (k_3 u_z^2 + k_1 u_x^2 + k_2 u_y^2)\bar{c}_\theta \quad (31)$$

All the terms in the right member in (31) are non-negative; therefore, $\mathbf{U}_{l2}$ is non-negative.

APPENDIX B
OBJECTIVE MEASURE TO ASSURE SLOWNESS

To provide an idea of objective measure to assure slowness, an analysis on the relation between motion slowness and contact constraints is given hereby. The Linear Inverted Pendulum Plus Flyweel Model (LIPPFM) proposed in [41] is adopted. This model abstracts a biped system as an inverted pendulum with an inertial flywheel centered at the CoM, which has a constant height of z_0. The equations of motion are

$$\begin{aligned} \ddot{x} &= \frac{g}{z_0}x - \frac{1}{mz_0}\tau_h \\ \ddot{\theta}_b &= \frac{1}{J}\tau_h \end{aligned} \quad (32)$$

where x and z are the CoM horizontal and vertical coordinates, θ_b is the flywheel angles with respect to vertical, g is the gravitational acceleration constant, m and J are the mass and the rotational inertia of the flywheel, and τ_h is the motor torque on the flywheel.

For non-sliding constraints, the ground reaction force (f_x, f_z) should remain inside a friction cone with a friction coefficient μ:

$$-\mu < \frac{f_x}{f_z} = \frac{x}{z_0} - \frac{\tau_h}{mgz_0} < \mu \quad (33)$$

which leads to the following constraint on x:

$$-\mu z_0 + \frac{\tau_h}{mg} < x < \mu z_0 + \frac{\tau_h}{mg}. \quad (34)$$

LIPPFM allows the robot to move one step to make the support polygon include x. However, here we need to find allowable motions which satisfy current foot contact constraints; so additionally, the CoM should be above the support polygon,
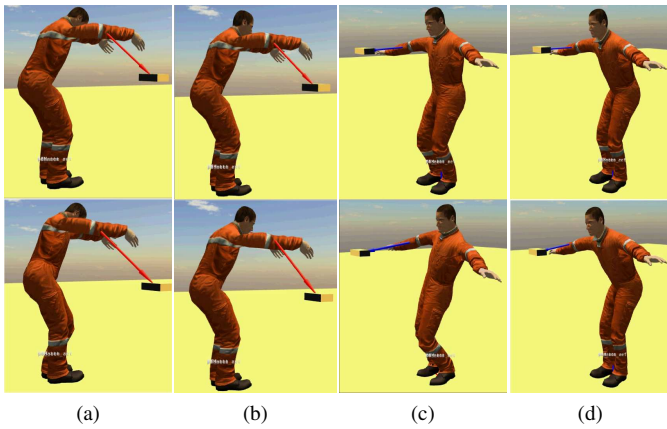

Fig. 10. Behaviors of the VH experiencing mechanical interactions with the environment. The VH was controlled by *Approach II* in (a) and (c), and by our approach in (b) and (d). Two tasks were performed: in (a) and (b), the VH was reaching its hands forward when the object was pulled $0.03m$ rightward and $0.1m$ downward; in (c) and (d), The VH was reaching its hands towards each side when the object was pulled $0.05m$ forward and $0.06m$ downward. The posture before (above) and after (below) being suddenly pulled by an elastic string of stiffness $500N.m^{-1}$ are depicted. The string is shown by the arrow which links the right arm with an object. When controlled by *Approach II*, the VH rotated its body with its arm pulling the string after perturbation.

Our approach is suitable for interactive applications such as virtual reality. It can work fast enough to allow the VH to interact with an operator and the virtual environment in real-time. With the application of wrench bounds, the operator can provide any reference motion without being worried about the VH's balance problem. The VH can perform a wide variety of tasks, such as reaching and manipulation. It can keep balance while trying to increase its workspace. The effectiveness of the proposed approach has been demonstrated by experiments. Full animations can be seen in the accompanying video.

For future research, we plan to work on more complex behaviors, such as manipulation during walking. These complex behaviors need motion planning, for which we plan to adopt predictive control [39,40] in our framework. We also plan to extend our method to handle multiple priority levels by the computation of a sequence of the maximum allowed potential energy associated with different priority levels.

APPENDIX A
THE ROTATIONAL POTENTIAL ENERGY

Here we prove the non-negative property of the rotational potential energy $\mathbf{U}_{l2}$ defined in (7). The rotational stiffness matrix and the associated co-stiffness matrix are denoted as $\mathbf{K}_{l2} = diag(k_1, k_2, k_3)$ and $\mathbf{G}_l = diag(g_1, g_2, g_3)$ respectively, with $k_i \geq 0, i = 1, 2, 3$, and $diag(a_1, ..., a_n)$ denoting a diagonal matrix whose diagonal entries starting in the upper left corner are $a_1, ..., a_n$. According to (8), we have

$$\begin{aligned} g_1 &= (k_2 + k_3 - k_1)/2, \\ g_2 &= (k_3 + k_1 - k_2)/2, \\ g_3 &= (k_1 + k_2 - k_3)/2. \end{aligned} \quad (27)$$

Without loss of generality, let $\mathbf{R} = \mathbf{R}_l^{-1}\mathbf{R}_l^d$ denote a matrix for a rotation by an angle of θ, about an axis in the direction

which provides bounds x_{min} and x_{max} for x. Finally x is constrained by

$$\max(-\mu z_0 + \frac{\tau_h}{mg}, \ x_{min}) < x < \min(\mu z_0 + \frac{\tau_h}{mg}, \ x_{max}). \tag{35}$$

From LIPPFM, the bounds on velocity $\dot{x}$ can be obtained. For example, with a step change in the rotational position of the flywheel of $\Delta\theta_b$, $\dot{x}$ is constrained by

$$\sqrt{\frac{g}{z_0}}(\underline{x} + \frac{J}{mz_0}\Delta\theta_{bmin}) < \dot{x} < \sqrt{\frac{g}{z_0}}(\bar{x} + \frac{J}{mz_0}\Delta\theta_{bmax}) \tag{36}$$

where $\underline{x}$ and $\bar{x}$ denote the lower and upper bounds of x.

With the above relations, an order of the magnitude of the maximum allowable motion velocity can be obtained. For example, consider a VH with a mass of $m = 79kg$, an inertia of $J = 3.125kgm^2$, the CoM height of $z_0 = 0.9m$, the minimum and maximum flywheel angle of $\Delta\theta_{bmin} = -\frac{1}{4}\pi$ and $\Delta\theta_{bmax} = \frac{3}{4}\pi$ respectively, the minimum and maximum CoM horizontal position of $x_{min} = -0.03m$ and $x_{max} = 0.06m$ respectively, and the minimum and maximum hip torque of $\tau_{hmin} = -100Nm$ and $\tau_{hmax} = 100Nm$ respectively. The friction coefficient between its foot and the ground is $\mu = 1$. The gravitational acceleration is $g = 9.81ms^{-2}$. According to (35), the lower and upper bounds of x are $\underline{x} = -0.03m$ and $\bar{x} = 0.06m$. Then according to (36), the lower and upper bounds of the velocity $\dot{x}$ are $\underline{\dot{x}} = -0.2ms^{-1}$ and $\bar{\dot{x}} = 0.5ms^{-1}$ respectively.

APPENDIX C
COMPUTATION OF THE ENERGY OF THE SYSTEM

The energy of the system at time $t \in [t_0, t_0 + T]$ can be obtained by the following computations. Substituting the expression of $\mathbf{W}_l$ (10) into (13) leads to

$$\mathbf{M}\dot{\mathbf{T}} + \mathbf{N}\mathbf{T} = -\mathbf{J}_0^T \nabla_{\mathbf{H}_0}\mathbf{U}_0 - \sum_{l \in \mathcal{L}} \alpha_l \mathbf{J}_l^T \nabla_{\mathbf{H}_l}\mathbf{U}_l$$
$$- (\mathbf{J}_0^T \mathbf{B}_0 \mathbf{J}_0 + \sum_{l \in \mathcal{L}} \mathbf{J}_l^T \mathbf{B}_l \mathbf{J}_l)\mathbf{T} \tag{37}$$
$$- \sum_k \mathbf{J}_{p_k}^T \mathbf{W}_{p_k}^r + \sum_j \mathbf{J}_{c_j}^T (\hat{\mathbf{F}}_{c_j} - \mathbf{F}_{c_j}^r).$$

Multiplying both sides of (37) with $-\mathbf{T}^T$ yields

$$-\mathbf{T}^T \mathbf{M}\dot{\mathbf{T}} - \mathbf{T}^T \mathbf{N}\mathbf{T} - \mathbf{T}^T(\mathbf{J}_0^T \mathbf{B}_0 \mathbf{J}_0 + \sum_{l \in \mathcal{L}} \mathbf{J}_l^T \mathbf{B}_l \mathbf{J}_l)\mathbf{T}$$
$$= \mathbf{V}_0^T \nabla_{\mathbf{H}_0}\mathbf{U}_0 + \sum_{l \in \mathcal{L}} \alpha_l \mathbf{V}_l^T \nabla_{\mathbf{H}_l}\mathbf{U}_l$$
$$+ \sum_k \mathbf{V}_{p_k}^T \mathbf{W}_{p_k}^r - \sum_j \mathbf{v}_{c_j}^T(\hat{\mathbf{F}}_{c_j} - \mathbf{F}_{c_j}^r)$$
$$= \frac{d\mathbf{U}_0}{dt} - \mathbf{V}_0^{d^T} \nabla_{\mathbf{H}_0^d}\mathbf{U}_0 \tag{38}$$
$$+ \sum_{l \in \mathcal{L}}(\frac{d(\alpha_l \mathbf{U}_l)}{dt} - \dot{\alpha}_l \mathbf{U}_l - \alpha_l \mathbf{V}_l^{d^T} \nabla_{\mathbf{H}_l^d}\mathbf{U}_l)$$
$$+ \sum_k \mathbf{V}_{p_k}^T \mathbf{W}_{p_k}^r - \sum_j \mathbf{v}_{c_j}^T(\hat{\mathbf{F}}_{c_j} - \mathbf{F}_{c_j}^r).$$

For no sliding contacts where the environment is fixed, the velocity $\mathbf{v}_{c_j} = 0$; thus we have

$$-\mathbf{T}^T \mathbf{M}\dot{\mathbf{T}} - \mathbf{T}^T \mathbf{N}\mathbf{T} - \mathbf{T}^T(\mathbf{J}_0^T \mathbf{B}_0 \mathbf{J}_0 + \sum_{l \in \mathcal{L}} \mathbf{J}_l^T \mathbf{B}_l \mathbf{J}_l)\mathbf{T}$$
$$= \frac{d\mathbf{U}_0}{dt} - \mathbf{V}_0^{d^T} \nabla_{\mathbf{H}_0^d}\mathbf{U}_0 + \sum_k \mathbf{V}_{p_k}^T \mathbf{W}_{p_k}^r \tag{39}$$
$$+ \sum_{l \in \mathcal{L}}(\frac{d(\alpha_l \mathbf{U}_l)}{dt} - \dot{\alpha}_l \mathbf{U}_l - \alpha_l \mathbf{V}_l^{d^T} \nabla_{\mathbf{H}_l^d}\mathbf{U}_l).$$

Integrating (39) with respect to time t yields (14).

REFERENCES

[1] D. Lee, C. Ott, and Y. Nakamura, "Mimetic communication model with compliant physical contact in human-humanoid interaction," *The International Journal of Robotics Research*, vol. 29, no. 13, pp. 1684–1704, 2010.

[2] B. L. Callennec and R. Boulic, "Interactive motion deformation with prioritized constraints," *Graphical Models*, vol. 68, no. 2, pp. 175–193, 2006.

[3] A. Shapiro, M. Kallmann, and P. Faloutsos, "Interactive motion correction and object manipulation," in *ACM SIGGRAPH*, ser. SIGGRAPH '08, 2008, pp. 57:1–57:8. [Online]. Available: http://doi.acm.org/10.1145/1401132.1401208

[4] S. Jain and C. K. Liu, "Interactive synthesis of human-object interaction," in *Proceedings of the 2009 ACM SIGGRAPH/Eurographics Symposium on Computer Animation*, ser. SCA '09, 2009, pp. 47–53.

[5] M. Liu, A. Micaelli, P. Evrard, A. Escande, and C. Andriot, "Interactive dynamics and balance of a virtual character during manipulation tasks," in *IEEE International Conference on Robotics and Automation (ICRA)*, may 2011, pp. 1676–1682.

[6] ——, "An energy based two level prioritized control for virtual humans," in *IEEE International Conference on Robotics and Biomimetics (ROBIO)*, dec. 2011, pp. 186–191.

[7] J. Pratt, A. Torres, P. Dilworth, and G. Pratt, "Virtual actuator control," in *IEEE/RSJ International Conference on Intelligent Robots and Systems (IROS)*, vol. 3, nov 1996, pp. 1219–1226.

[8] S. Coros, P. Beaudoin, and M. van de Panne, "Generalized biped walking control," *ACM Trans. Graph.*, vol. 29, pp. 130:1–130:9, July 2010.

[9] E. Demircan, L. Sentis, V. Sapio, and O. Khatib, "Human motion reconstruction by direct control of marker trajectories," in *Advances in Robot Kinematics: Analysis and Design*. Springer Netherlands, 2008, pp. 263–272.

[10] O. Khatib, L. Sentis, and J.-H. Park, "A unified framework for whole-body humanoid robot control with multiple constraints and contacts," in *European Robotics Symposium 2008*, ser. Springer Tracts in Advanced Robotics. Springer Berlin / Heidelberg, 2008, vol. 44, pp. 303–312.

[11] J.-c. Wu and Z. Popović, "Terrain-adaptive bipedal locomotion control," *ACM Trans. Graph.*, vol. 29, pp. 72:1–72:10, July 2010.

[12] B. Stephens and C. Atkeson, "Dynamic balance force control for compliant humanoid robots," in *IEEE/RSJ International Conference on Intelligent Robots and Systems (IROS)*, oct. 2010, pp. 1248–1255.

[13] A. Liégeois, "Automatic supervisory control of the configuration and behavior of multibody mechanisms," *IEEE Transactions on Systems, Man and Cybernetics*, vol. 7, no. 12, pp. 868–871, dec. 1977.

[14] L. Sentis and O. Khatib, "Task-oriented control of humanoid robots through prioritization," in *IEEE RAS/RSJ International Conference on Humanoid Robots*, 2004.

[15] E. Yoshida, M. Poirier, J.-P. Laumond, O. Kanoun, F. Lamiraux, R. Alami, and K. Yokoi, "Pivoting based manipulation by a humanoid robot," *Autonomous Robots*, vol. 28, pp. 77–88, 2010.

[16] O. Khatib, L. Sentis, J. Park, and J. Warren, "Whole-body dynamic behavior and control of human-like robots," *I. J. Humanoid Robotics*, vol. 1, no. 1, pp. 29–43, 2004.

[17] D. Raunhardt and R. Boulic, "Immersive singularity-free full-body interactions with reduced marker set," *Computer Animation and Virtual Worlds*, 2011. [Online]. Available: http://dx.doi.org/10.1002/cav.378

[18] O. Khatib, "Real-time obstacle avoidance for manipulators and mobile robots," *The International Journal of Robotics Research*, vol. 5, no. 1, pp. 90–98, 1986.

[19] L. Sentis and O. Khatib, "Control of free-floating humanoid robots through task prioritization," in *IEEE International Conference on Robotics and Automation (ICRA)*, april 2005, pp. 1718–1723.

[20] O. Stasse, A. Escande, N. Mansard, S. Miossec, P. Evrard, and A. Kheddar, "Real-time (self)-collision avoidance task on a hrp-2 humanoid robot," in *IEEE International Conference on Robotics and Automation (ICRA)*, may 2008, pp. 3200–3205.

[21] L. Saab, P. Soueres, and J. Fourquet, "Coupling manipulation and locomotion tasks for a humanoid robot," in *International Conference on Advances in Computational Tools for Engineering Applications (ACTEA)*, july 2009, pp. 84–89.

[22] N. Mansard, O. Khatib, and A. Kheddar, "A unified approach to integrate unilateral constraints in the stack of tasks," *IEEE Transactions on Robotics*, vol. 25, no. 3, pp. 670–685, june 2009.

[23] O. Kanoun, F. Lamiraux, P.-B. Wieber, F. Kanehiro, E. Yoshida, and J.-P. Laumond, "Prioritizing linear equality and inequality systems: Application to local motion planning for redundant robots," in *IEEE International Conference on Robotics and Automation (2009)*, may 2009, pp. 2939–2944.

[24] A. Escande, N. Mansard, and P.-B. Wieber, "Fast resolution of hierarchized inverse kinematics with inequality constraints," in *IEEE International Conference on Robotics and Automation (ICRA)*, may 2010, pp. 3733–3738.

[25] L. Saab, N. Mansard, F. Keith, J.-Y. Fourquet, and P. Soueres, "Generation of dynamic motion for anthropomorphic systems under prioritized equality and inequality constraints," in *IEEE International Conference on Robotics and Automation (ICRA)*, may 2011, pp. 1091–1096.

[26] O. Kanoun, F. Lamiraux, and P.-B. Wieber, "Kinematic control of redundant manipulators: Generalizing the task-priority framework to inequality task," *IEEE Transactions on Robotics*, vol. 27, no. 4, pp. 785–792, aug. 2011.

[27] A. Rennuit, A. Micaelli, X. Merlhiot, C. Andriot, F. Guillaume, N. Chevassus, D. Chablat, and P. Chedmail, "Passive control architecture for virtual humans," in *IEEE/RSJ International Conference on Intelligent Robots and Systems (IROS)*, aug. 2005, pp. 1432–1437.

[28] A. Rennuit, "Contribution au contrôle des humains virtuels interactifs," *PhD thesis, Ecole Centrale de Nantes*, pp. 73–77, 2006, in French.

[29] B. Hannaford and J.-H. Ryu, "Time-domain passivity control of haptic interfaces," *IEEE Transactions on Robotics and Automation*, vol. 18, no. 1, pp. 1–10, feb 2002.

[30] J.-P. Kim and J. Ryu, "Robustly stable haptic interaction control using an energy-bounding algorithm," *The International Journal of Robotics Research*, vol. 29, no. 6, pp. 666–679, 2010.

[31] J. Krüger and D. Surdilovic, "Robust control of force-coupled human-robot-interaction in assembly processes," *CIRP Annals - Manufacturing Technology*, vol. 57, no. 1, pp. 41–44, 2008.

[32] E. Colgate and N. Hogan, "The interaction of robots with passive environments: Application to force feedback control," in *Fourth International Conference on Advanced Robotics*, 1989.

[33] Y. Abe, M. da Silva, and J. Popović, "Multiobjective control with frictional contacts," in *Proceedings of the ACM SIGGRAPH/Eurographics symposium on Computer animation*, 2007, pp. 249–258.

[34] C. Collette, A. Micaelli, C. Andriot, and P. Lemerle, "Dynamic balance control of humanoids for multiple grasps and non coplanar frictional contacts," in *7th IEEE-RAS International Conference on Humanoid Robots*, 2007, pp. 81–88.

[35] E. D. Fasse and P. C. Breedveld, "Modeling of elastically coupled bodies: Part i—general theory and geometric potential function method," *Journal of Dynamic Systems, Measurement, and Control*, vol. 120, no. 4, pp. 496–500, 1998.

[36] M. Spong and F. Bullo, "Controlled symmetries and passive walking," *IEEE Transactions on Automatic Control*, vol. 50, no. 7, pp. 1025–1031, july 2005.

[37] R. Chipalkatty and M. Egerstedt, "Human-in-the-loop: Terminal constraint receding horizon control with human inputs," in *2010 IEEE International Conference on Robotics and Automation (ICRA)*, may 2010, pp. 2712–2717.

[38] L. Sentis, J. Park, and O. Khatib, "Compliant control of multicontact and center-of-mass behaviors in humanoid robots," *IEEE Transactions on Robotics*, vol. 26, no. 3, pp. 483–501, june 2010.

[39] U. Muico, Y. Lee, J. Popović, and Z. Popović, "Contact-aware nonlinear control of dynamic characters," *ACM Trans. Graph.*, vol. 28, pp. 81:1–81:9, July 2009.

[40] M. Da Silva, Y. Abe, and J. Popović, "Simulation of human motion data using short-horizon model-predictive control," *Computer Graphics Forum*, vol. 27, no. 2, pp. 371–380, 2008.

[41] J. Pratt, J. Carff, S. Drakunov, and A. Goswami, "Capture point: A step toward humanoid push recovery," in *Humanoid Robots, 2006 6th IEEE-RAS International Conference on*, dec. 2006, pp. 200 –207.

Mingxing Liu received the M.S. degrees in engineering in 2009 from Ecole Centrale Paris, France and from Shanghai Jiao Tong University, China. She is a Ph.D. candidate at Université Pierre et Marie Curie, Paris, France. She is currently working toward the Ph.D. degree at the Systems and Technologies Integration Laboratory of the French Atomic Energy Commission (CEA-LIST). Her current research interests include automatic control, whole-body control for virtual humans, and human-robot interaction.

Alain Micaelli was born in Ajaccio, France, in 1956. He received the Engineer and the Ph.D. degrees in automatic control and signal processing in 1979 and 1982, respectively, from the Ecole Nationale Supérieure des Télécommunications, Paris, France, and from the University of Paris-Sud, France. He joined the Robotics Unit of the French Atomic Energy Commission (CEA) in 1982 and has been involved in several national and international projects dealing with teleoperation and mobile robotics. He is now Research Director in the field of automatic control. His research interests include the control of manipulators, telemanipulators, mobile robots, virtual reality and more specifically virtual manikin.

Paul Evrard received a M.S. degree in computer science in 2006 from Institut d'Informatique d'Entreprise, France and a PhD degree in 2010 in robotics from Universit de Montpellier 2, France. He is currently a research scientist at CEA-LIST at Fontenay-aux-Roses, France. His research interests include digital human modelling and control, humanoid robotics and human-robot interaction.

Adrien Escande received the M.S. degree in 2005 from Ecole des Mines de Paris, Paris, France and the Ph.D. degree in 2008 in robotics from Universit d'Evry Val-d'Essonne, Evry, France after spending three years in the Joint Japenese-French Robotics Laboratory (JRL) in Tsukuba, Japan. Since then, he has been working as a research scientist in CEA-LIST at Fontenay-aux-Roses, France. His current research interests include whole-body planning and control for humanoid robots and mathematical optimization for robotics.

Claude Andriot received the PhD degree in robotics from the University of Paris 6 in 1992. He is currently at CEA (French nuclear authority) in the Robotics and Interactive Systems Technologies Lab. He is the CEA project leader of the Perfrv platform (French Platform on Virtual Reality, http://www.perfrv.org). His research activities and projects involve control of force feedback devices for desktop and nuclear applications, control of wearable haptic interfaces for virtual reality, and real time physical simulation of mechanical systems.